



Cite this: *Nanoscale*, 2017, 9, 6886

Highly efficient oxygen evolution from CoS₂/CNT nanocomposites *via* a one-step electrochemical deposition and dissolution method†

Jizhang Yang,^a Zhi Yang,^{id} *^a Lu Hua Li,^{id} ^b Qiran Cai,^b Huagui Nie,^a Mengzhan Ge,^a Xi'an Chen,^{id} ^a Ying Chen^b and Shaoming Huang^{*a,c}

The oxygen evolution reaction (OER) has been viewed as a critical step in electrochemical energy conversion and storage devices. However, searching for cheap and efficient OER electrocatalysts still remains an urgent task. Herein, we develop a new strategy involving a one-step electrochemical deposition and dissolution method to fabricate hydrophilic porous CoS₂/carbon nanotube (CNT) composites (CNT-CoS₂). X-ray photoelectron spectroscopy and near-edge X-ray absorption fine structure spectroscopy measurements confirm the formation of hydrophilic groups on the surface of the porous CoS₂ during electrochemical oxidation. Our design holds several advantages. The electricity conductivity of CoS₂ is increased by introducing CNTs as a conductive substrate. The porous nanostructures of CoS₂ increase its surface area, and provide paths to promote charge and reactant transfer. The active edge sites modified with hydrophilic groups can increase the content of electrolyte–electrode contact points, increasing the intrinsic catalytic performance of CoS₂. These factors allow CNT-CoS₂ to achieve a low onset potential of 1.33 V vs. RHE, a stable current density (*j*) of 10 mA cm⁻² at an overpotential of 290 mV, and excellent stability under alkaline conditions compared to that of IrO₂. The comprehensive performance of the CNT-CoS₂ electrocatalyst is comparable to or better than that of any reported noble metal-free OER catalyst, even RuO₂ and IrO₂. This facile synthesis strategy involving synchronous electrochemical deposition and dissolution should be easily adapted for large-scale water electrolysis.

Received 24th February 2017,

Accepted 17th April 2017

DOI: 10.1039/c7nr01293d

rsc.li/nanoscale

Introduction

The oxygen evolution reaction (OER) is one of the half reactions of water splitting, and is considered a critical step in electrochemical energy conversion and storage devices such as metal–air batteries and fuel cells, and water electrolysis.^{1–5} In alkaline solution, the OER is a multistep, four-electron process and suffers from sluggish kinetics and high overpotential. Efficient OER catalysts are desired to address these challenges. To date, the most effective electrocatalysts for the OER are RuO₂ and IrO₂,⁶ but their high cost, low abundance, and instability hinder their large-scale applications. Tremendous effort has been made to the development of highly active,

stable, and low-cost nonprecious metal catalysts (*e.g.*, Ni,⁷ Co,^{8,9} and Fe¹⁰ based compounds). Among these catalysts, half-metallic CoS₂, an earth-abundant mineral,¹¹ shows great potential as an alternative to RuO₂ and IrO₂ because of its appreciable conductivity (6.7 × 10³ S cm⁻¹ at 300 K), which exceeds those of other semiconducting transition metal disulfides such as FeS₂ and NiS₂,¹² and noble metal-like catalytic properties.¹³ However, in view of the inherent physical and chemical properties of CoS₂, three attributes must be optimized to achieve the desired OER performance: (1) conductivity and diffusion properties need to be enhanced;¹⁴ (2) the number of active sites and their intrinsic activity should be increased; and (3) interfacial wettability must be improved. Point (3) is required because improvement of the wetting behavior of CoS₂ towards the OER can increase the electrolyte–electrode contact points, facilitating electron transfer, and thus enhancing electrocatalytic activity.

Recent drives to develop CoS₂-based electrocatalysts have primarily focused on coupling CoS₂ materials with conductive carbon nanostructures, developing nanoscale structures to increase the exposure of active sites, and engineering the active edge sites to facilitate the intrinsic activity of CoS₂ by

^aNanomaterials & Chemistry Key Laboratory, Wenzhou University, Wenzhou, 325027, P. R. China. E-mail: yang201079@126.com, smhuang@wzu.edu.cn

^bInstitute for Frontier Materials, Deakin University, Waurn Ponds, Victoria, 3216, Australia

^cSchool of Material and Energy, Guangdong University of Technology, Guangzhou, 510006, P. R. China

† Electronic supplementary information (ESI) available. See DOI: 10.1039/c7nr01293d

doping with other transition metals.^{15–19} Although these approaches do improve the activity of CoS₂ towards the OER, most reported CoS₂-based electrocatalysts have not reached the efficiency of RuO₂ and IrO₂ ones. After comprehensively analyzing these aforementioned strategies, we infer that the main reason for the limited progress of CoS₂-based electrocatalysts may be because these previous studies only optimized one or two of the three required attributes detailed above. Little research aimed at improving the wettability of CoS₂ has been proposed.

Herein, we develop a new strategy involving a one-step electrochemical deposition and dissolution method to fabricate porous CoS₂/carbon nanotube (CNT) composites (denoted as CNT-CoS₂). We use X-ray photoelectron spectroscopy (XPS) and near-edge X-ray absorption fine structure spectroscopy (NEXAFS) to confirm the formation of hydrophilic groups on the surface of the porous CoS₂ during electrochemical oxidation. Our design holds several advantages. The electrical conductivity of CoS₂ is increased by introducing CNTs as a conductive substrate. The porous nanostructures of CoS₂ have increased surface area, which provides paths to promote charge and reactant transfer. It is also confirmed that the active edge sites modified with hydrophilic groups can increase the content of electrolyte–electrode contact points, increasing the intrinsic catalytic performance of CoS₂. These factors allow CNT-CoS₂ to achieve a low onset potential of 1.33 V *vs.* RHE, a stable current density (*j*) of 10 mA cm⁻² at an overpotential of 290 mV, and excellent stability under alkaline conditions comparable to that of IrO₂. The comprehensive performance of the CNT-CoS₂ electrocatalyst is on par with or better than that of any reported noble metal-free OER catalyst, even RuO₂ and IrO₂. This facile synthesis strategy involving one-step electrochemical deposition and dissolution should be easily adapted for large-scale water electrolysis.

Experimental details

Materials

Potassium hydroxide, barium chloride and ammonium hydroxide were purchased from Guangdong Xilong Chemical Factory. And the above reagents are analytically pure. Thiourea (AR, 99%) and iridium oxide (99.9% metal basis, Ir ≥84.5%) were purchased from Aladdin. Potassium chloride (AR) was purchased from Zhejiang Zhongxing Chemical Factory. Cobalt chloride hexahydrate (AR) was purchased from Shanghai Sinopharm Chemical Reagent Co., Ltd.

Electrode preparation

Glassy carbon (GC) electrodes (5 mm diameter, CH Instruments Inc.) were polished with 0.05 μm alumina slurry (CH Instruments Inc.) and subsequently rinsed with ultrapure water and ethanol. The electrodes were then sonicated in ultrapure water and ethanol, and dried under a gentle nitrogen stream. To prepare the working electrode, 2 mg CNT was ultrasonically dispersed in 500 μL ethanol and deionized water (the

volume ratio of ethanol and deionized water is 4 : 1), and 10 μL suspension were dropped onto the GC surface and dried at room temperature. For comparison, a commercially available IrO₂-modified GCE was prepared in the same way.

Synthesis of cobalt disulfide nanosheet

CNT-CoS₂ hybrids were synthesized using a facile electrochemical deposition method. The electrodynamic deposition was carried out in a three-electrode cell using a cleaned glassy carbon electrode as the working electrode, Pt as the counter electrode, and Ag/AgCl (saturated-KCl) as the reference electrode by cyclic voltammetry. In short, the CNT-modified glass carbon electrodes were placed in the electrolyte solution containing a certain concentration of cobalt chloride hexahydrate (CoCl₂·6H₂O) and thiourea (CS(NH₂)₂), and electrodeposited at a potential range between 0.2 and -1.2 V *vs.* Ag/AgCl under cyclic voltammograms (CV) at a scan rate of 30 mV s⁻¹. The pH value of the electrolyte was adjusted with diluted NH₃H₂O to ≈6, because CoOOH and Co₃O₄ form as intermediates or as final products of oxidation in neutral and basic media.^{20,21} At the end of deposition, the working electrode was rinsed with water gently and dried under vacuum at room temperature overnight. For comparison, bare glass carbon electrodes without CNTs were treated under the same synthesis conditions, and parallel experiments using various deposition cycles were also carried out. The obtained hybrids were denoted as CNT-CoS₂-20, CNT-CoS₂-40, CNT-CoS₂-60, CNT-CoS₂-80, and CNT-CoS₂-120 according to various deposition cyclic numbers, respectively.

Electrochemical measurements

Electrochemical measurements were performed at room temperature using a rotating disk working electrode made of glassy carbon (PINE, 5 mm diameter, 0.196 cm²) connected to a Multipotentiostat (PINE, Grove City, America). A standard three-electrode electrochemical cell filled with a 0.1 M KOH electrolyte, CNT-CoS₂-modified glass carbon electrodes as the working electrode, Ag/AgCl (saturated-KCl) and Pt sheet electrodes as the reference electrode and the counter electrode, respectively was used. All of the potentials in our manuscript are calibrated to a reversible hydrogen electrode (RHE) based on the Nernst equation.

Before the electrochemical measurement, the electrolyte (0.1 M KOH, pH ~ 13) was degassed by bubbling O₂ for 30 min. The polarization curves were obtained by sweeping the potential from 0 to 0.8 V *vs.* Ag/AgCl, with a scan rate of 5 mV s⁻¹ and 1600 rpm. The data were recorded after applying a number of potential sweeps until they were stable.

The accelerated stability tests were performed in O₂-saturated 0.1 M KOH at room temperature by potential cycling between 0.3 and 0.8 V *vs.* Ag/AgCl at a sweep rate of 100 mV s⁻¹ for 1000 cycles. At the end of the cycles, the resulting electrode was used for OER polarization by sweeping the potential from 0 to 0.8 V *vs.* Ag/AgCl, with a sweep rate of 5 mV s⁻¹ and 1600 rpm. Chronoamperometry curves were recorded at a 10 mA cm⁻² over 36 000 s at room temperature.

Tafel plots were obtained from LSV curves for assessment of the OER activities of investigated catalysts. According to the Tafel equation ($\eta = b \log(j) + a$), the Tafel slope (b) can be obtained by fitting the linear portion of the Tafel plots into it.

The electrochemical surface area (ECSA) was determined by measuring the capacitive current associated with double-layer charging from the scan-rate dependence of CVs. For this, the potential window of CVs was 0.2–0.3 V *vs.* Ag/AgCl. The scan rates were 20, 40, 60, 80, 100 and 120 mV s⁻¹. The double layer capacitance (C_{dl}) was estimated by plotting the $\Delta j = (j_a - j_c)$ at 0.25 V *vs.* Ag/AgCl against the scan rate. The linear slope is twice that of the double layer capacitance C_{dl} .

Structure characterization

X-ray photoelectron spectroscopy (XPS) measurements were carried out with an ultrahigh vacuum setup, equipped with a monochromatic Al K α X-ray source and a high resolution Gammadata-Scienta SES 2002 analyzer. Scanning electron microscopy (SEM) images were obtained with a JSM-6700F field-emission scanning electron microscope. Transmission electron microscopy (TEM) and high-resolution transmission electron microscopy (HRTEM) images were recorded with a JEOL-3010 instrument. The NEXAFS measurements were performed in the ultra-high vacuum chamber at the undulator soft X-ray spectroscopy beamline of the Australian Synchrotron, Victoria, Australia. The photon energy was corrected by the photoelectron current of the beam measured on an Au grid.

Results and discussion

Fig. 1 outlines the one-step electrochemical deposition and dissolution procedure used to synthesize CNT-CoS₂. The hybrid catalysts were synthesized *via* a one-step electrochemical process wherein CNT-modified glassy carbon electrodes (CNT-modified GCEs) were immersed in the electrolyte containing cobalt chloride hexahydrate and thiourea and then subjected to potential cycling. Scanning from 0.2 to -1.2 V *vs.* Ag/AgCl caused cathodic peaks to emerge that likely originate

from the reduction and co-precipitation of cobalt and sulfur as CoS₂ (Fig. S1A, ESI[†]). Scanning in the opposite direction from -1.2 to 0.2 V *vs.* Ag/AgCl resulted in anodic peaks attributed to the oxidation and dissolution of the CoS₂ film. For comparison, a bare GCE (denoted as bare.elec+60) was also cycled under the same conditions. Because of the importance of deposition cycle number (n) on CoS₂ formation, parallel experiments using $n = 20, 40, 60, 80$ and 120 were conducted, giving hybrid catalysts denoted as CNT-CoS₂-20, CNT-CoS₂-40, CNT-CoS₂-60, CNT-CoS₂-80, and CNT-CoS₂-120, respectively. Data for these catalysts are summarized in Table S1.[†]

The scanning electron microscopy (SEM) and transmission electron microscopy (TEM) images in Fig. 2A and B show that CNT-CoS₂-60 contains sheet structures uniformly interspersed into the CNT network. Fig. 2C and S2E[†] illustrate a scanning transmission electron microscopy (STEM) image and the corresponding energy-dispersive X-ray (EDX) elemental mappings, revealing uniform distributions of S, Co, and O atoms in the sheet structure. Typical TEM images (Fig. 2D–F, and S2A–D, ESI[†]) indicate that the sheet structures contain numerous pores with a diameter of 10–20 nm. The HRTEM images in Fig. S2D[†] and Fig. 2D, E show typical lattice fringes with fringe spacings of 0.32, 0.27, and 0.54 nm for the framework of the

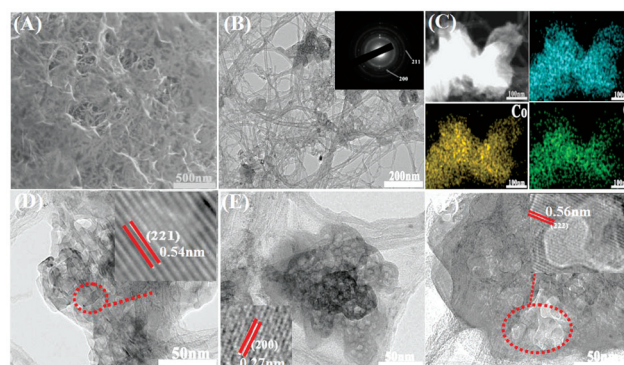


Fig. 2 Structural characterization of an as-synthesized CNT-CoS₂-60 hybrid catalyst: (A) SEM images; (B) TEM images; (C) STEM and corresponding elemental mapping; (D–F) HRTEM.

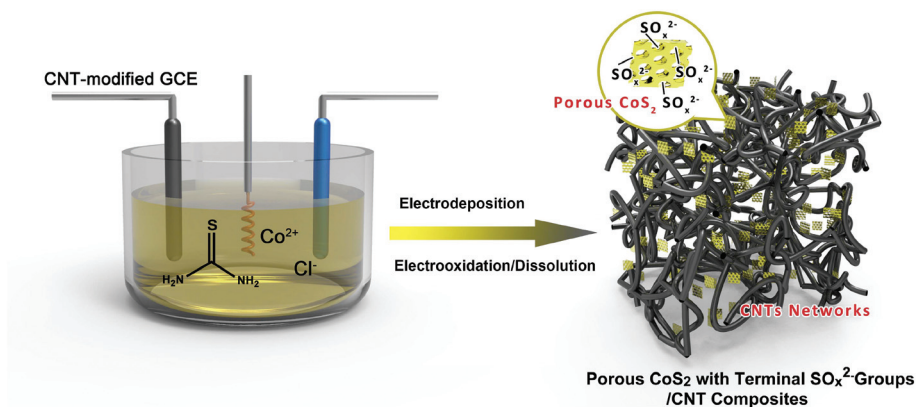


Fig. 1 A schematic diagram to illustrate the operating principle of the OER based on CNT-CoS₂ nanocomposites.

sheet structure, consistent with the spacing of the (111),²² (200),²³ and (221) planes of CoS₂ (PDF # 65-3322), respectively. These results also agree well with the corresponding selected-area electron diffraction pattern (inset of Fig. 2B), confirming the presence of CoS₂ on the CNTs. Also, from Fig. 2F, a lattice fringe with a spacing of 0.56 nm can be seen on the edge of the pore structures. After combining with the subsequent observations of XPS and NEXAFS, it was speculated that the lattice fringe of 0.56 nm may be attributed to the (222) planes of CoSO₄, which could originate from oxidation of CoS₂ during the electrochemical process.

XPS was used to investigate the chemical composition of CNT-CoS₂. The survey spectrum of CNT-CoS₂-60 (Fig. S3A, ESI†) contained C 1s, O 1s, Co 2p and S 2p peaks, further con-

firmed the presence of elemental S, Co, and O. This is also consistent with the EDX spectrum for CNT-CoS₂-60 (Fig. S2F, ESI†). The S 2p peak from 161.8 to 165.1 eV (Fig. S3B, ESI†) suggests the existence of S-S or S-Co,²⁴ while the S 2p peak observed at ~169.1 eV is attributed to surface sulfur with a high oxidation state. NEXAFS at S K-edge, Co L-edge and O K-edge was used to gain more insights into the chemical environment. The S K-edge (Fig. 3A) shows two broad peaks representing reduced (S_{Red}) and oxidized (S_{Ox}) S species. The S_{Red} peak at 2473.4 eV is attributed to S₂²⁻, while the S_{Ox} peaks from 2477.1 to 2483.5 eV can be split into sulfone (-SO₂), sulfonate (-SO₃)²⁵ and sulfate (SO₄²⁻) contributions.²⁶ According to XPS, CNT-CoS₂-60 displayed Co-related peaks at 782.1 and 798.0 eV attributed to Co²⁺ configurations (Fig. S4, ESI†).^{27,28}

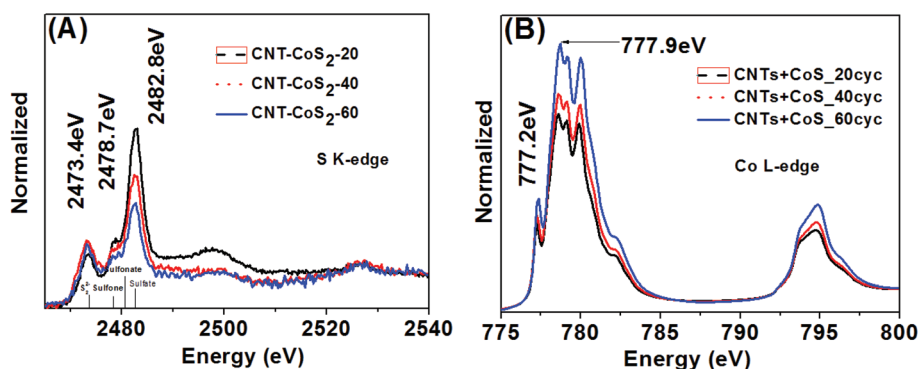


Fig. 3 Near-edge X-ray absorption fine structure spectroscopy (NEXAFS) characterization: (A) S K-edge; (B) Co L-edge.

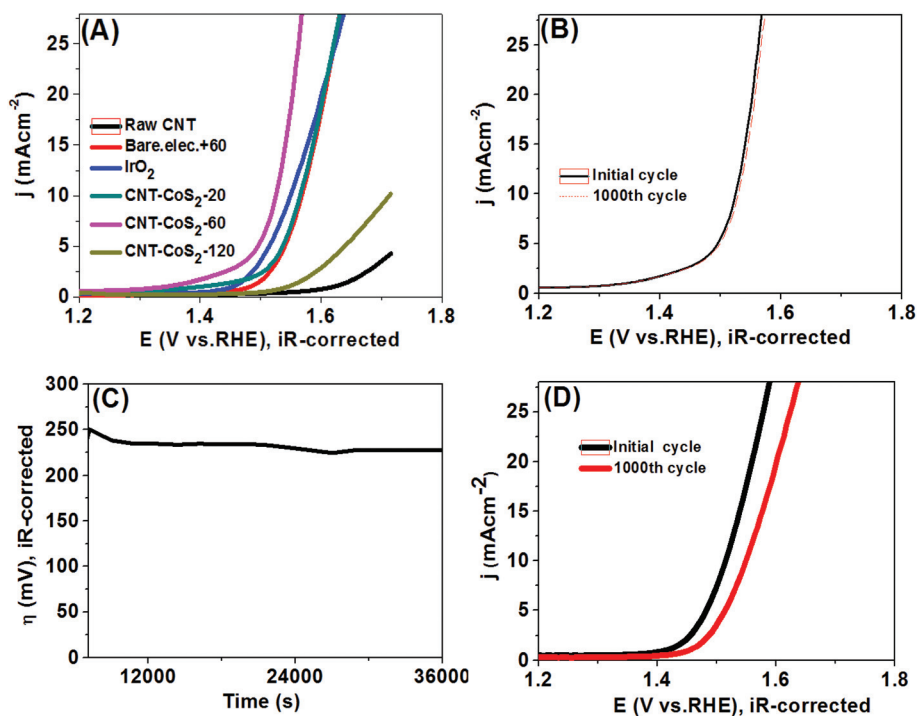


Fig. 4 (A) *iR*-Corrected polarization curves for different deposition cycles and raw CNT, bare.elec.-CoS₂-60, IrO₂ in KOH solution (0.1 M); (B) *iR*-corrected polarization curves of CNT-CoS₂-60 initially and after 1000 CV scans at 100 mV s⁻¹; (C) *iR*-corrected chronopotentiometry curve of CNT-CoS₂-60; and (D) *iR*-corrected polarization curves of IrO₂ initially and after 1000 CV scans at 100 mV s⁻¹.

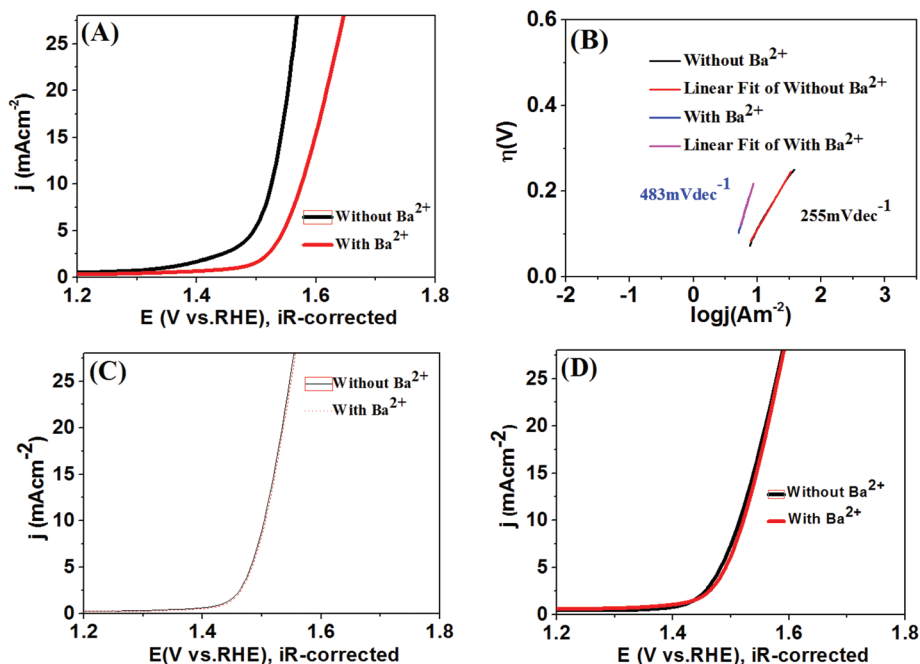
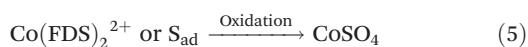
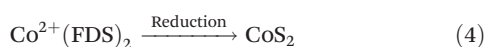
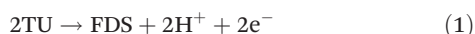


Fig. 5 (A) OER *iR*-corrected polarization plots of CNT-CoS₂-60 in 0.1 M KOH with Ba²⁺; (B) *iR*-corrected Tafel plots of (A); (C) *iR*-corrected polarization curves of the CNT/commercial CoS₂ hybrid; and (D) OER *iR*-corrected polarization plots of IrO₂ in 0.1 M OH with Ba²⁺.

Additionally, the structure of NEXAFS spectra in the Co L-edge region of depositions after different cycles is similar (Fig. 3B), and Co possessed an average oxidation state of +2 in the CNT-CoS₂-60 sample, consistent with the XPS analysis above. The O K-edge NEXAFS data prove that the state of O in CNT-CoS₂-60 was different from that of the raw CNTs, indicating that O in CNT-CoS₂-60 is derived from the electrochemical synthesis process rather than the raw CNTs (Fig. S5B, ESI†).²⁹ Overall, the aforementioned analyses coupled with the TEM observation in Fig. 2F confirm that the terminal S atoms in the porous CoS₂ were oxidized to form hydrophilic groups (*e.g.*, SO₄²⁻ and SO₃²⁻) during the electrochemical process. The measurement result of contact angles (Fig. S6, ESI†) further showed that the wettability of the CNT-CoS₂-60 was superior to that of the CNT/commercial CoS₂ (Alfa Aesar, 99.5%) composites.



Meanwhile, the two anodic peaks in Fig. S1A† likely reflected the oxidation of CoS₂ and formation of soluble CoSO_x (eqn (5) and (6)),^{30,31} which facilitated the formation of terminal hydrophilic groups in the porous CoS₂, accelerating the

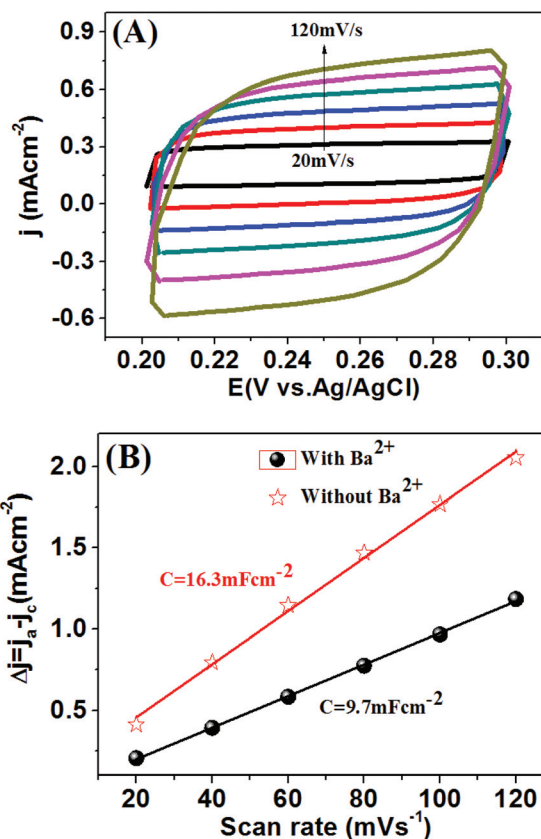


Fig. 6 (A) CVs at different scan rates in a potential window where no Faradaic processes occur (0.2–0.3 V vs. Ag/AgCl) for CNT-CoS₂-60 in 0.1 M KOH with Ba²⁺; and (B) charging current density differences ($\Delta j = j_a - j_c$) plotted against scan rates.

dissolution of reaction products from the reaction interface to the electrolyte and pore formation (Fig. 2D–F and S2A–C, ESI†). The formation of terminal hydrophilic groups has seldom been mentioned, even in previous research using very similar electrochemical conditions. After consideration of the cyclic voltammetry (CV) curves reported by Yang's group,³² which were attributed to the electrodeposition of CoS_x on fluorine-doped tin oxide (FTO), we speculate that the unique anodic peak II at ~ 0.1 V vs. Ag/AgCl, which only appeared in our case, may represent the formation of terminal hydrophilic groups. We believe that the excellent conductivity of the CNTs, which exceeds that of FTO or other substrates, plays an important role in promoting the formation of terminal hydrophilic groups in porous CoS_2 . To obtain further insight into the role of cobalt ions in the formation of porous CoS_2 , the same CV cycles were performed under similar conditions using TU and potassium chloride instead of cobalt chloride. Fig. S1B and C† reveal that a similar curve containing two anodic peaks and

two reduction peaks was obtained, indicating that hydrophilic group formation was not influenced by the cobalt ions. This result is also consistent with the aforementioned XPS and NEXAFS findings.

The OER activity of CNT- CoS_2 was evaluated under alkaline conditions (0.1 M KOH) with a typical three-electrode configuration. GCEs modified with a constant active mass loading of raw CNTs, CNT- CoS_2 , bare.elec+60, and IrO_2 were used as working electrodes. As a typical reference metric for electrochemical catalytic performance, CNT- CoS_2 -60 achieved a small onset voltage of 1.33 V vs. RHE (Fig. 4A and S7A in ESI†) and a stable j of 10 mA cm^{-2} at an overpotential of 290 mV. These values are better than those of IrO_2 and most reported state-of-the-art noble metal-free OER catalysts (e.g. $\text{Ni}_2\text{Co}_1/\text{Ni}_2\text{Co}_1\text{O}_x$, Co_3S_4 nanosheet, $\text{Co}_9\text{S}_8/\text{MoS}_2/\text{CNF}$, Table S2 in ESI†). Furthermore, the Tafel slopes were also obtained from the polarization curve, and a Tafel slope of 255 mV per decade was measured for CNT- CoS_2 -60 (Fig. S7B, ESI†).

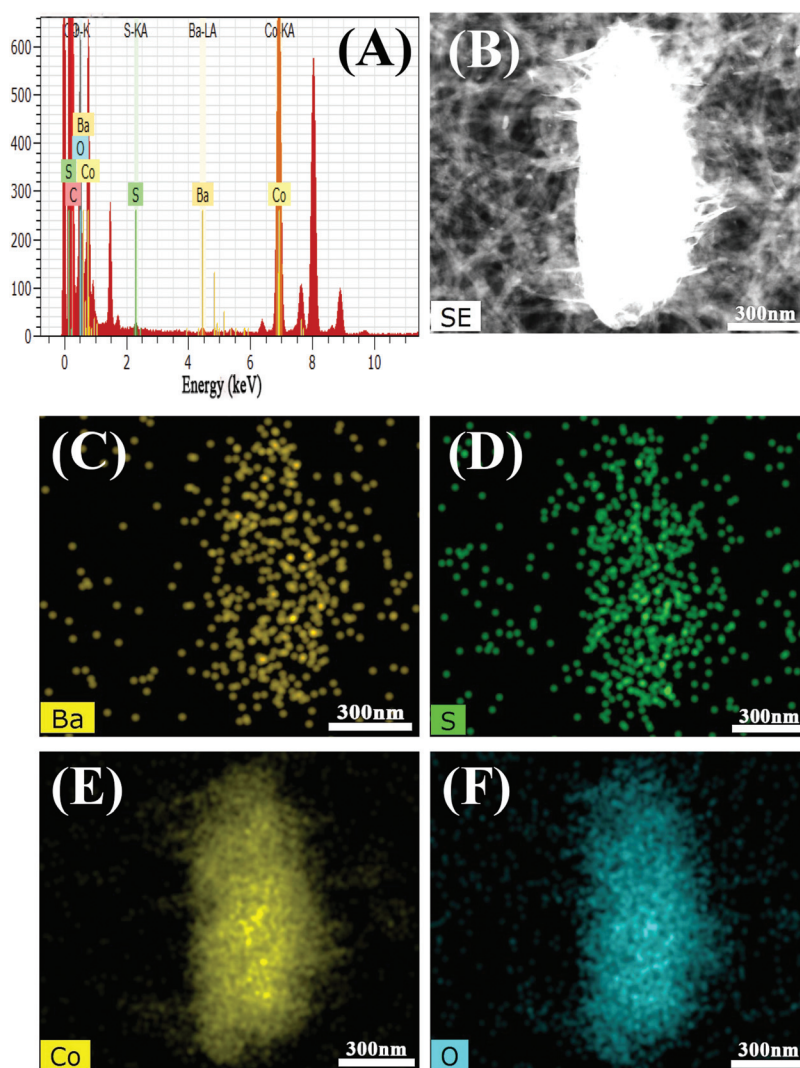


Fig. 7 (A) EDX of CNT- CoS_2 -60 dipped in 0.1 M KOH with Ba^{2+} ; (B–F) STEM and the corresponding elemental mapping of the CNT- CoS_2 -60 hybrid dipped in 0.1 M KOH with Ba^{2+} .

The CNT-CoS₂-60 catalyst demonstrated a more negative onset potential and higher catalytic current than those of the bare.elec+60 or CNT electrode (Fig. 4A and S7A, ESI†). These experimental results indicate that a positive synergistic effect is obtained following hybridization of CoS₂ with CNTs, which enhances OER activity. Furthermore, CNT-CoS₂-60 exhibited the most negative onset potential and the highest catalytic current of all the CNT-CoS₂ samples. Therefore, the activity of these CNT-CoS₂ hybrid catalysts is sensitive to *n*.

To further investigate the effect of *n* on the OER activity of the CNT-CoS₂ catalysts, we performed electrochemical impedance spectroscopy (EIS) in 10 mM KOH. The obtained Nyquist plots are presented in Fig. S8A,† and the electrical equivalent circuit diagram shown in Fig. S8B† was used to model the solid-liquid interface after the experimental data were well fitted. Furthermore, Fig. S8C† was used to demonstrate the accuracy of the fitting process. The impedance parameters obtained by fitting the EIS responses are listed in Table S3.† CNT-CoS₂-60 has a low charge transfer resistance (*R*_{ct}), and the largest constant phase element (CPE) value among the CNT-CoS₂ catalysts. A low *R*_{ct} value indicates faster surface charge transfer and a higher reaction rate in electrocatalysis. Meanwhile, a large CPE value corresponds to a high active surface area, which can strongly enhance OER performance. These may be the main reasons that CNT-CoS₂-60 displays the highest OER activity of the CNT-CoS₂ catalysts. In other words, the varying activity of these catalysts may result from their different loading and surface electrocatalysis kinetics. The CNT-CoS₂ nanocomposites with *n* < 60 are expected to have fewer active sites than those with larger *n*. Conversely, *n* > 60 may lead to increased CoS₂ thickness (Fig. S9 and S10, ESI†), thus decreasing the density of the edge active sites and increasing *R*_{ct}.

The long-term cycling stability of CNT-CoS₂-60 was assessed by performing continuous CV for 1000 cycles. For comparison, the stability of IrO₂ under the same conditions was also determined. The polarization curve of CNT-CoS₂-60 after 1000 cycles overlaid almost exactly with the initial one (Fig. 4B), suggesting the catalyst is highly stable and can withstand accelerated degradation. The durability of CNT-CoS₂-60 was higher than that of commercial IrO₂ (Fig. 4D). Fig. 4C shows that the chronoamperometry measurement response for CNT-CoS₂-60 remained relatively constant for at least 36 000 s. The excellent long-term stability of CNT-CoS₂-60 suggests that it is attractive for potential applications.

To further investigate the nature of the active sites of CNT-CoS₂-60, we designed an experiment to measure the influence of SO_x²⁻ (*x* = 2, 3 and 4) on its OER activity. Polarization curves of CNT-CoS₂-60 were obtained in KOH solutions with and without Ba²⁺, wherein the pH values for the two KOH solutions are equal. Fig. 5A reveals that the overpotential of CNT-CoS₂-60 increased markedly to ~40 mV at a current density of 10 mA cm⁻². Kinetic results also confirmed that the catalytic performance of CNT-CoS₂-60 degraded upon introducing Ba²⁺ (Fig. 5B, ESI†). It is believed that the reason for the decreased catalytic performance may be due to the fact that

Ba²⁺ forms complexes with sulfate in CoS₂, hindering diffusion of the bath solution and bulk O₂ at the catalyst-electrolyte interface, limiting the OER reaction process.

To further determine the reason, we measured the double layer capacitance (*C*_{dl}) of the electrode with and without Ba²⁺. Fig. 6A and B show that *C*_{dl} obviously decreased after immersion in Ba²⁺. These results also agree well with the corresponding observations of EDX and STEM as shown in Fig. 7. Similar measurements for CNT/commercial CoS₂ composites and IrO₂-modified GCEs were also conducted for comparison. Fig. 5C and D show that their overpotentials at a current density of 10 mA cm⁻² did not clearly vary upon addition of Ba²⁺, implying that Ba²⁺ did not affect the catalytic activity of commercial CoS₂ and IrO₂. The above-mentioned results demonstrate that the terminal hydrophilic groups (SO_x²⁻, *x* = 2, 3 and 4) and the porous structure in CNT-CoS₂-60 formed by the electrooxidation and electrodisolution reaction play important roles in promoting charge and reactant transport as well as increasing intrinsic OER activity.

To further understand the effect of Co²⁺ in the OER, we investigated the influence of thiocyanate ions (SCN⁻) on the OER activity of CNT-CoS₂-60. SCN⁻ is widely known to poison

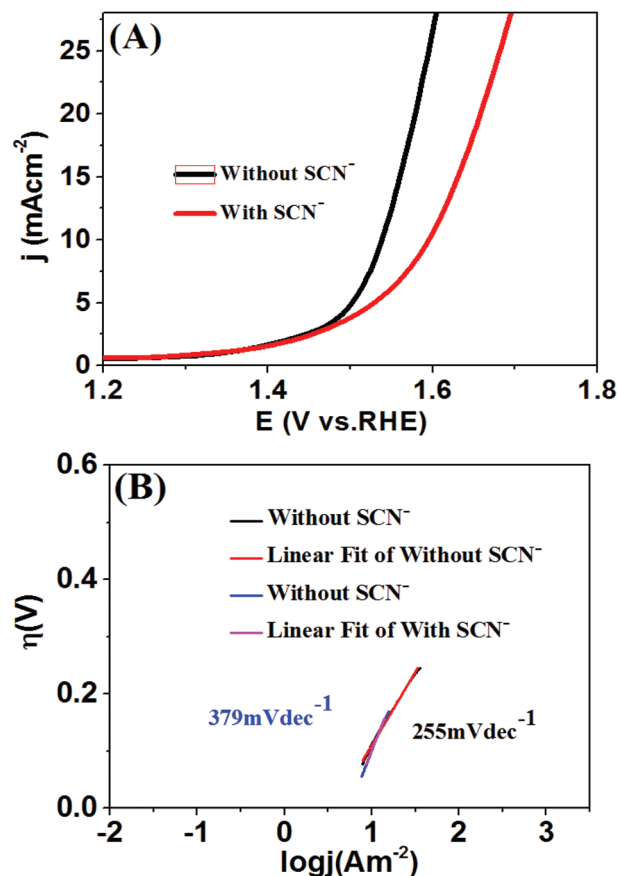


Fig. 8 (A) OER *iR*-corrected polarization plots of CNT-CoS₂-60 in 0.1 M KOH with SCN⁻, indicating that SCN⁻ ions strongly poison the CNT-CoS₂-60. These measurements indicated that the cobalt is partially involved in the active centers. (B) *iR*-Corrected Tafel plots of (A).

metal-centered catalytic sites under alkaline conditions.³³ Upon introducing SCN^- into 0.1 M KOH, the overpotential increased to ~ 50 mV at 10 mA cm^{-2} (Fig. 8A and S11, ESI†), which suggests that some cobalt sites were blocked. The kinetic analysis shown in Fig. 8B also supports this observation. These results strongly indicate that Co^{2+} is a catalytic site in the OER catalyzed by CNT- CoS_2 -60.

Conclusions

In summary, a one-step electrochemical deposition and dissolution process was used to synthesize composites consisting of CNTs and porous CoS_2 with terminal hydrophilic groups. CNTs, a support material with negligible OER activity, coupled well with CoS_2 to accelerate electron transfer and promote the OER activity. CNTs also served as an effective support to mediate the surface performance of CoS_2 by promoting the formation of hydrophilic groups. These factors allow the as-prepared porous CoS_2 with terminal hydrophilic groups achieve a low onset potential of 1.33 V vs. RHE, a stable current density of 10 mA cm^{-2} at an overpotential of 290 mV, and excellent stability under alkaline conditions. We attribute its high activity to the porous structure providing numerous active sites and paths to promote both charge and reactant transfer. The terminal hydrophilic groups introduced during the electrooxidation process enhanced the hydrophilicity of materials, increasing both the number of electrolyte-electrode contact points and intrinsic catalytic performance of CoS_2 . The facile nature, versatility, and scalability of this approach mean that it has great potential to produce nanocomposites for use in other catalytic and optoelectronic applications.

Acknowledgements

The work was supported in part by grants from NSFC (51572197, 21273163, 21475096 and 51420105002) and the State Key Laboratory of Structural Chemistry (20170035). This research was undertaken on the soft X-ray beamline at the Australian Synchrotron, Victoria, Australia. The authors thank Dr Dingyi Tong for designing the TOC graphic.

References

- 1 L. Xu, Q. Q. Jiang, Z. H. Xiao, X. Y. Li, J. Huo, S. Y. Wang and L. M. Dai, Plasma-Engraved Co_3O_4 Nanosheets with Oxygen Vacancies and High Surface Area for the Oxygen Evolution Reaction, *Angew. Chem., Int. Ed.*, 2016, **55**, 5277–5281.
- 2 T. Ling, D. Y. Yan, Y. Jiao, H. Wang, Y. Zheng, X. L. Zheng, J. Mao, X. W. Du, Z. P. Hu, M. Jaroniec and S. Z. Qiao, Engineering Surface Atomic Structure of Single-crystal Cobalt(II) Oxide Nanorods for Superior Electrocatalysis, *Nat. Commun.*, 2016, **7**, 12876.
- 3 C. Tang, H. S. Wang, H. F. Wang, Q. Zhang, G. L. Tian, J. Q. Nie and F. Wei, Spatially Confined Hybridization of Nanometer-Sized NiFe Hydroxides into Nitrogen-Doped Graphene Frameworks Leading to Superior Oxygen Evolution Reactivity, *Adv. Mater.*, 2015, **27**, 4516–4522.
- 4 Y. W. Wang, B. Z. Wang, F. Gu, Z. H. Zheng and J. J. Liu, Tuning Electrochemical Reactions in Li- O_2 Batteries, *Nano Adv.*, 2016, **1**, 17.
- 5 S. Dou, L. Tao, J. Huo, S. Y. Wang and L. M. Dai, Etched and Doped Co_9S_8 /Graphene Hybrid for Oxygen Electrocatalysis, *Energy Environ. Sci.*, 2016, **9**, 1320–1326.
- 6 X. W. Yu, M. Zhang, J. Chen, Y. R. Li and G. Q. Shi, Nitrogen and Sulfur Codoped Graphite Foam as a Self-Supported Metal-Free Electrocatalytic Electrode for Water Oxidation, *Adv. Energy Mater.*, 2016, **6**, 1501492.
- 7 M. R. Gao, W. C. Sheng, Z. B. Zhuang, Q. R. Fang, S. Gu, J. Jiang and Y. S. Yan, Efficient Water Oxidation Using Nanostructured alpha-Nickel-Hydroxide as an Electrocatalyst, *J. Am. Chem. Soc.*, 2014, **136**, 7077–7084.
- 8 X. Liu, W. Liu, M. Ko, M. J. Park, M. G. Kim, P. Oh, S. J. Chae, S. Park, A. Casimir, G. Wu and J. Cho, Metal (Ni, Co)-Metal Oxides/Graphene Nanocomposites as Multifunctional Electrocatalysts, *Adv. Funct. Mater.*, 2015, **25**, 5799–5808.
- 9 C. W. Tung, Y. Y. Hsu, Y. P. Shen, Y. X. Zheng, T. S. Chan, H. S. Sheu, Y. C. Cheng and H. M. Chen, Reversible Adapting Layer Produces Robust Single-Crystal Electrocatalyst for Oxygen Evolution, *Nat. Commun.*, 2015, **6**, 8106.
- 10 M. Gong, Y. G. Li, H. L. Wang, Y. Y. Liang, J. Z. Wu and J. G. Zhou, An Advanced Ni-Fe Layered Double Hydroxide Electrocatalyst for Water Oxidation, *J. Am. Chem. Soc.*, 2013, **135**, 8452–8455.
- 11 M. S. Faber, R. Dziedzic, M. A. Lukowski, N. S. Kaiser, Q. Ding and S. Jin, High-Performance Electrocatalysis Using Metallic Cobalt Pyrite (CoS_2) Micro- and Nanostructures, *J. Am. Chem. Soc.*, 2014, **136**, 10053–10061.
- 12 Z. Yuan, H. J. Peng, T. Z. Hou, J. Q. Huang, C. M. Chen, D. W. Wang, X. B. Cheng, F. Wei and Q. Zhang, Powering Lithium-Sulfur Battery Performance by Propelling Polysulfide Redox at Sulfiphilic Hosts, *Nano Lett.*, 2016, **16**, 519–527.
- 13 M. R. Gao, Y. F. Xu, J. Jiang and S. H. Yu, Nanostructured Metal Chalcogenides: Synthesis, Modification, and Applications in Energy Conversion and Storage Devices, *Chem. Soc. Rev.*, 2013, **42**, 2986–3017.
- 14 G. F. Chen, T. Y. Ma, Z. Q. Liu, N. Li, Y. Z. Su, K. Davey and S. Z. Qiao, Efficient and Stable Bifunctional Electrocatalysts Ni/NixMy (M = P, S) for Overall Water Splitting, *Adv. Funct. Mater.*, 2016, **26**, 3314–3323.
- 15 J. H. Wang, W. Cui, Q. Liu, Z. C. Xing, A. M. Asiri and X. P. Sun, Recent Progress in Cobalt-Based Heterogeneous Catalysts for Electrochemical Water Splitting, *Adv. Mater.*, 2016, **28**, 215–230.
- 16 P. Ganesan, M. Prabu, J. Sanetuntikul and S. Shanmugam, Cobalt Sulfide Nanoparticles Grown on Nitrogen and

- Sulfur Codoped Graphene Oxide: An Efficient Electrocatalyst for Oxygen Reduction and Evolution Reactions, *ACS Catal.*, 2015, 5, 3625–3637.
- 17 Y. W. Liu, C. Xiao, M. J. Lyu, Y. Lin, W. Z. Cai, P. C. Huang, W. Tong, Y. M. Zou and Y. Xie, Ultrathin Co_3S_4 Nanosheets that Synergistically Engineer Spin States and Exposed Polyhedra that Promote Water Oxidation under Neutral Conditions, *Angew. Chem., Int. Ed.*, 2015, 54, 1–6.
 - 18 A. Sivanantham, P. Ganesan and S. Shanmugam, Hierarchical NiCo_2S_4 Nanowire Arrays Supported on Ni Foam: An Efficient and Durable Bifunctional Electrocatalyst for Oxygen and Hydrogen Evolution Reactions, *Adv. Funct. Mater.*, 2016, 26, 4661–4672.
 - 19 X. F. Liu, Ionothermal Synthesis of Carbon Nanostructures: Playing with Carbon Chemistry in Inorganic Salt Melt, *Nano Adv.*, 2016, 1, 90.
 - 20 Y. J. Sun, C. Liu, D. C. Grauer, J. Yano, J. R. Long, P. D. Yang and C. J. Chang, Electrodeposited Cobalt-Sulfide Catalyst for Electrochemical and Photoelectrochemical Hydrogen Generation from Water, *J. Am. Chem. Soc.*, 2013, 135, 17699–17702.
 - 21 W. A. Badawy, F. M. Al-Kharafi and J. R. Al-Ajmi, Electrochemical Behaviour of Cobalt in Aqueous Solutions of Different pH, *J. Appl. Electrochem.*, 2000, 30, 693–704.
 - 22 F. Song, X. L. Hu and J. Chang, Ultrathin Cobalt-Manganese Layered Double Hydroxide Is an Efficient Oxygen Evolution Catalyst, *J. Am. Chem. Soc.*, 2014, 136, 16481–16484.
 - 23 S. J. Peng, L. L. Li, X. P. Han, W. P. Sun, M. Srinivasan, S. G. Mhaisalkar, F. Y. Cheng, Q. Y. Yan, J. Chen and S. Ramakrishna, Cobalt Sulfide Nanosheet/Graphene/Carbon Nanotube Nanocomposites as Flexible Electrodes for Hydrogen Evolution, *Angew. Chem., Int. Ed.*, 2014, 53, 12594–12599.
 - 24 Z. Peng, D. S. Jia, A. M. Al-Enizi, A. A. Elzatahry and G. F. Zheng, From Water Oxidation to Reduction: Homologous Ni-Co Based Nanowires as Complementary Water Splitting Electrocatalysts, *Adv. Energy Mater.*, 2015, 5, 1402031.
 - 25 A. M. El-Sawy, I. M. Mosa, D. Su, C. J. Guild, S. Khalid, R. Joesten, J. F. Rusling and S. L. Suib, Controlling the Active Sites of Sulfur-Doped Carbon Nanotube-Graphene Nanolobes for Highly Efficient Oxygen Evolution and Reduction Catalysis, *Adv. Energy Mater.*, 2016, 6, 1501966.
 - 26 F. Jalilehvand, Sulfur: not a “Silent” Element any more, *Chem. Soc. Rev.*, 2006, 35, 1256–1268.
 - 27 L. Fu, Z. Liu, Y. Liu, B. Han, P. Hu, L. Cao and D. Zhu, Beaded Cobalt Oxide Nanoparticles along Carbon Nanotubes: Towards More Highly Integrated Electronic Devices, *Adv. Mater.*, 2005, 17, 217–221.
 - 28 H. F. Wang, C. Tang, X. L. Zhu and Q. Zhang, A ‘Point-Line-Point’ Hybrid Electrocatalyst for Bi-functional Catalysis of Oxygen Evolution and Reduction Reactions, *J. Mater. Chem. A*, 2016, 4, 3379–3385.
 - 29 E. C. Todd, D. M. Sherman and J. A. Purton, Surface Oxidation of Chalcopyrite (CuFeS_2) under Ambient Atmospheric and Aqueous (pH 2–10) Conditions: Cu, Fe L- and O K-edge X-ray Spectroscopy, *Geochim. Cosmochim. Acta*, 2003, 67, 2137–2146.
 - 30 A. E. Bolzan, P. L. Schilardi, R. C. V. Piatti, T. Iwasita, A. Cuesta, C. Guti-errez and A. J. Arvia, Comparative Voltammetric and FTIRRAS Study on the Electro-oxidation of Thiourea and Methyl-thioureas on Platinum in Aqueous acid Solutions, *J. Electroanal. Chem.*, 2004, 571, 59–72.
 - 31 A. E. Bolzan, R. C. V. Piatti, R. C. Salvarezza and A. J. Arvia, Electrochemical Study of Thiourea and Substituted Thiourea Adsorbates on Polycrystalline Platinum Electrodes in Aqueous Sulfuric Acid, *J. Appl. Electrochem.*, 2002, 32, 611–620.
 - 32 N. Kornienko, J. Resasco, N. Becknell, C. M. Jiang, Y. S. Liu, K. Q. Nie, X. H. Sun, J. H. Guo, S. R. Leone and P. D. Yang, Operando Spectroscopic Analysis of an Amorphous Cobalt Sulfide Hydrogen Evolution Electrocatalyst, *J. Am. Chem. Soc.*, 2015, 137, 7448–7455.
 - 33 H. W. Liang, S. Brüller, R. H. Dong, J. Zhang, X. L. Feng and K. Mullen, Molecular Metal-Nx Centres in Porous Carbon for Electrocatalytic Hydrogen Evolution, *Nat. Commun.*, 2015, 6, 7992.